Distance dependence of energy transfer from InGaN quantum wells to graphene oxide

T. N. Lin,[1] L. T. Huang,[1] G. W. Shu,[1] C. T. Yuan,[1] J. L. Shen,[1,*] C. A. J. Lin,[2] W. H. Chang,[2] C. H. Chiu,[3] D. W. Lin,[3] C. C. Lin,[3] and H. C. Kuo[3]

[1]*Department of Physics and Institute of Biomedical Technology, Chung Yuan Christian University, Chung-Li, Taiwan*

[2]*Department of Biomedical Engineering and Institute of Biomedical Technology, Chung Yuan Christian University, Chung-Li, Taiwan*

[3]*Department of Photonic and Institute of Electro-Optical Engineering, National Chiao Tung University, Hsin-Chu, Taiwan*

**Corresponding author: jlshen@cycu.edu.tw*

Received February 27, 2013; revised June 25, 2013; accepted June 26, 2013;
posted July 11, 2013 (Doc. ID 186038); published July 31, 2013

We report the distance-dependent energy transfer from an InGaN quantum well to graphene oxide (GO) by time-resolved photoluminescence (PL). A pronounced shortening of the PL decay time in the InGaN quantum well was observed when interacting with GO. The nature of the energy-transfer process has been analyzed, and we find the energy-transfer efficiency depends on the $1/d^2$ separation distance, which is dominated by the layer-to-layer dipole coupling.

OCIS codes: (260.2160) Energy transfer; (300.6500) Spectroscopy, time-resolved.
http://dx.doi.org/10.1364/OL.38.002897

Förster resonance energy transfer (FRET), in which a fluorescent donor transfers energy to a fluorescent or nonfluorescent acceptor via nonradiative dipole–dipole interaction, has important applications in biomedical analysis and optoelectronics [1–3]. In traditional FRET, both the donor and the acceptor are dye molecules and the donor–acceptor interactions are often limited by the need for overlap between the emission and absorption spectra. Recently, attempts have been made to use nanomaterials as novel donors and/or acceptors [4–8]. Quantum dots (QDs), which provide remarkable optical properties, have been employed as the energy donors to participate in FRET [4,5]. The broad excitation spectra and large absorption cross section of QDs permit flexibility in the selection of the donor excitation wavelength. On the other hand, metal nanoparticles have been explored as the efficient acceptors to substitute for organic acceptors [6,7]. The fluorescence quenching of donor molecules in close proximity to metal nanoparticles has been found to follow the $1/d^4$ distance dependence (d is the distance between the donor and the acceptor), referred to the nanometal surface energy transfer (NSET) [6,7]. While NSET is similar to FRET, in that the interaction is dipole–dipole energy transfer in nature, it is geometrically different from FRET. NSET has been accounted for by a point dipole interacting with the infinite metal surface [4,7]. Very recently, graphene and its partially oxidized form graphene oxide (GO) have been used as efficient acceptors i, and the rate of energy transfer from the localized point-like molecule to graphene has been found to have a $1/d^4$ distance [8–13]. Graphene-based FRET has gained considerable interest due to the exploration of new limits of light–matter interactions [10–12]. So far, graphene and GO have been used as FRET acceptors paired with organic dyes or QDs as donors. However, little attention has been given to an energy-transfer system between the quantum well (QW) and graphene (or GO). Because of their size-tunable optical properties and excellent resistance to photobleaching, QWs are expected to be efficient donors. This suggest that QWs and graphene (or GO) could provide good donor–acceptor pairs. In this Letter, we propose an energy-transfer system, in which the InGaN QW acts as the donor and GO act as the acceptor (Fig. 1). Such energy transfer was characterized by the time-resolved photoluminescence (PL). Distance-dependent interactions of InGaN QWs and GO were studied to analyze the mechanism of the energy-transfer processes.

The donor used for the present study is a single InGaN/GaN QW structure grown by metal-organic chemical vapor deposition on a sapphire substrate. After a 2 μm thick GaN buffer layer on the substrate, a single InGaN QW layer with thickness of 2 nm was grown. The growth is terminated by the GaN cap layer with different thicknesses to control the separation between donors and acceptors. The cap layer thicknesses of six samples were 2, 4, 6, 8, 12, and 20 nm. The acceptor GO was purchased from *Graphene Supermarket* (USA). The GO consists of a single graphene sheet, and its concentration is 275 mg/L. The thickness of GO flakes is one atomic layer (at least 80%), and the size of GO flakes is 0.5–5 μm [14]. To perform the experiment, GO was incorporated on the top of the QW cap layer by the drop-casting method. The steady-state and time-resolved PL was measured at room temperature. A pulsed laser with a wavelength of 260 nm, a repetition frequency of 20 MHz, and a duration of 250 fs was used as the excitation source. The collected luminescence was projected into a spectrometer and detected with a high-speed photomultiplier tube (PMT).

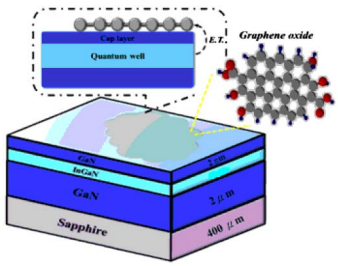

Fig. 1. Schematic representation of the energy transfer from a InGaN QW to GO.

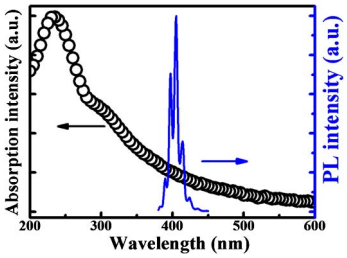

Fig. 2. Absorption spectrum of GO (open circles) and PL spectrum of the InGaN QW (solid line).

Time-resolved PL were performed using the technique of time-correlated single-photon counting (TCSPC).

The open circles in Fig. 2 show the optical absorption spectrum of the GO, displaying a broadband absorption from the near-infrared to the ultraviolet region. A clear maximum at ~233 nm is ascribed to $\pi - \pi^*$ transition of the C – C aromatic rings, and the shoulder at ~300 nm is ascribed to $n - \pi^*$ transition of C = O bonds [15]. The appearance of the characteristic peak is in agreement with previous reports [15].

The solid line in Fig. 2 shows the PL of the InGaN QW with a cap thickness of 2 nm. The PL reveals a narrow PL band that peaks at around 405 nm. To demonstrate the energy transfer from QWs to GO, the PL decays of the bare QW and the hybrid structure (i.e., QWs plus GO) were measured. Figure 3 shows the PL decay curves of QWs without (open circles) and with (open triangles) GO for some samples. As shown in Fig. 3, reduction of the QW lifetime after introducing the GO confirms the presence of an additional decay channel owing to energy transfer. The PL decay of the InGaN QW is expected to be characterized by a distribution of lifetimes owing to the indium phase segregation and the indium fluctuation [16]. Thus, all the PL decay curves in Fig. 3 were fitted by the stretched exponential function:

$$n(t) = n(0)e^{-(kt)^{\beta}}, \tag{1}$$

where $n(t)$ are carrier densities, k is the decay rate of carriers, and is a dispersive exponent. Fitting parameters were automatically obtained by fitting the stretched exponential function to the experimental data. The corresponding parameters obtained from the fits are given in Table 1. The solid lines in Fig. 3 show the fitted curves using Eq. (3), replicating well with the experimental

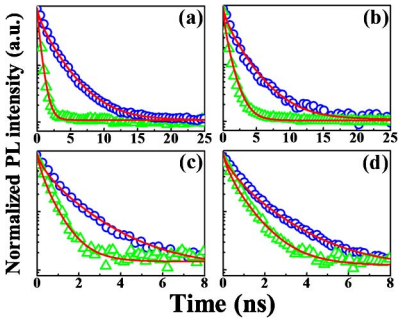

Fig. 3. PL decay profiles of InGaN QW in the absence (open circles) and presence (open triangles) of GO with a cap thickness of (a) 2 nm, (b) 4 nm, (c) 6 nm, and (d) 8 nm. The solid lines are the fitted curves using Eq. (1).

Table 1. Dispersion Components β, Decay Rates k, and Average Decay Times $\langle\tau\rangle$ Obtained from the PL Decays in Fig. 3

	Without GO			With GO		
Cap Thickness (nm)	β	k (ns^{-1})	$\langle\tau\rangle$ (ns)	β (ns)	k (ns^{-1})	$\langle\tau\rangle$
2	0.735	0.77	1.58	0.736	4.35	0.37
4	0.730	0.76	1.59	0.733	2.38	0.51
6	0.731	1.42	0.86	0.727	3.33	0.37
8	0.727	1.30	0.90	0.728	2.22	0.55

results. In the stretched exponential function, the average decay time is calculated as follows [17]:

$$\langle t\rangle = \frac{1}{k\beta}\Gamma\left(\frac{1}{\beta}\right), \tag{2}$$

where Γ is the mathematical gamma function. The calculated average decay time $\langle t\rangle$ for the PL decays in Fig. 3 is displayed in Table 1.

In the absence of GO, the PL decay time of the bare QW can be represented by $\langle\tau_{QW}\rangle$. After introducing GO, the PL decay of the QW is described by the following equation:

$$\langle\tau_{hybrid}\rangle^{-1} = \langle\tau_{QW}\rangle^{-1} + \langle\tau_{ET}\rangle^{-1}, \tag{3}$$

where $\langle\tau_{ET}\rangle$ represents the characteristic time of the energy-transfer process. Thus, the corresponding energy-transfer rate $\langle K_{ET}\rangle = \langle\tau_{ET}\rangle^{-1}$ can be determined using Eq. (3). The energy-transfer efficiency Φ_{ET} is the fraction of the photons absorbed by the donor that are transferred to the acceptor and can be expressed by

$$\Phi_{ET} = \frac{\langle K_{ET}\rangle}{\langle\tau_{QW}\rangle^{-1} + \langle K_{ET}\rangle}. \tag{4}$$

Φ_{ET} as a function of cap thickness was obtained according to Eq. (4) and displayed as the solid circles in Fig. 4. Φ_{ET} decreases monotonically with the increase of the cap thickness in InGaN QWs. The maximum energy-transfer efficiency obtained from experiment is as high as 82% for the InGaN QW with a cap thickness of 2 nm. The high energy-transfer efficiency indicates a higher signal-to-background ratio and thus better sensitivity and a greater dynamic range for the sensing applications. It is noted that charge transfer through tunneling from

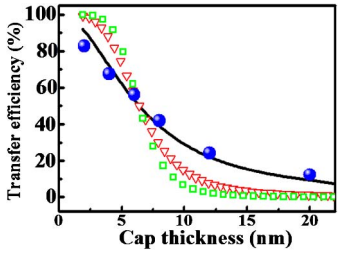

Fig. 4. Experimental data points (solid circles) and theoretical fits of the energy-transfer efficiency versus the cap thickness. The solid line, open triangles, and open squares are the fitted curves using Eq. (6) with $n = 2$, 4, and 6, respectively.

donors to acceptors may also contribute to the shortening of the PL decay. However, if charge transfer is the dominant process, the transfer efficiency should decay exponentially with cap thickness. In our experiments the dependence of transfer efficiency on the cap thickness (solid circles in Fig. 3) does not follow the exponential decay law. We therefore suggest that charge transfer is not the dominant factor in our system. Nevertheless, we cannot rule out the possibility that charge transfer may exist and contribute to the measured PL decay. In particular, when the cap thickness approaches zero, charge transfer is expected to have some contribution in the PL decay.

In the traditional FRET mechanism, the energy-transfer rate exhibits a d^{-6} dependence. However, when either the donor or the acceptor or both are extended systems with delocalized charge densities, the non-d^{-6} of the energy-transfer rate occurs [13]. The ratio of the energy transfer and QW decay rates is expected to depend on d according to [18]

$$\langle K_{\mathrm{ET}}\rangle/\langle \tau_{\mathrm{QW}}\rangle^{-1} = (d_0/d)^n, \tag{5}$$

where d_0 is the donor-to-acceptor distance at which the energy-transfer efficiency is 50%. d_0 is associated with the length scale for detection of energy transfer. The larger d_0, the larger the detectable distance for an energy-transfer system. From Fig. 4, d_0 is estimated to be ~6.4 nm, close to the Förster radius of the energy transfer between InGaN QWs and polyfluorene (~6.1 nm) [18]. n is a parameter that depends on the nature of the dipole–dipole interaction. $n = 6$, 4, and 2 represent the interactions from point dipoles to point dipoles (FRET), point dipoles to two-dimensional dipoles (NSET), and two-dimensional dipoles to two-dimensional dipoles, respectively [18]. Combining Eqs. (4) and (5), the energy-transfer efficiency can be written as [7]

$$\Phi_{\mathrm{ET}} = \frac{1}{1 + (d/d_0)^n}. \tag{6}$$

Taking $d_0 = 6.4$ nm, comparison of the experimental Φ_{ET} with the fitted result for $n = 6$ (open squares), $n = 4$ (open triangles), and $n = 2$ (solid line) is shown in Fig. 4. FRET ($n = 6$) and NSET ($n = 4$) fail to predict the experimental energy-transfer efficiency in the present system. On the other hand, the fit with $n = 2$ dependence is in good agreement with the experimental result. The $n = 2$ dependence corresponds to the nature of layer-to-layer dipole coupling, suggesting that the energy transfer from InGaN QWs to GO reveals a layer-to-layer coupling process. The $1/d^2$ dependence of energy transfer allows a longer detection distance than that with FRET and NSET. Thus, this type of energy transfer can be a useful spectroscopic ruler for determining the relative distance in thin films. For example, energy-transfer efficiency can provide a probe to detect the bilayer formation or interlayer mixing in self-assembled thin films [19].

In summary, we have demonstrated an energy transfer from InGaN QWs to GO by observing a shortening of the PL decay time for the InGaN QW in the presence of GO. The energy-transfer efficiency follows a $1/d^2$ dependence on the distance between the InGaN QW and GO, suggesting a layer-to-layer dipole coupling. The energy-transfer efficiency of this type can be as high as 82%, which is promising for developing the sensing applications.

This project was supported in part by Chung Yuan Christian University and the National Science Council under Grant Nos. NSC 100-2112-M-033-005-MY3 and NSC101-2627-M-033-002.

References

1. T. Förster, Ann. Phys. **437**, 55 (1948).
2. J. R. Lakowicz, *Principle of Fluorescence Spectroscopy*, 2nd ed. (Kluwer Academic Plenum, 1999).
3. V. M. Agranovich, Y. N. Gartstein, and M. Litinskaya, Chem. Rev. **111**, 5179 (2011).
4. T. Pons, I. L. Medintz, K. E. Sapsford, S. Higashiya, A. F. Grimes, D. S. English, and H. Matoussi, Nano Lett. **7**, 3157 (2007).
5. S. Sadhu, K. K. Haldar, and A. Patra, J. Phys. Chem. C **114**, 3891 (2010).
6. S. Saraswat, A. Desireddy, D. Zheng, L. Guo, H. P. Lu, T. P. Bigioni, and D. Isailovic, J. Phys. Chem. C **115**, 17587 (2011).
7. M. Prabha and G. F. Strouse, J. Am. Chem. Soc. **132**, 9383 (2010).
8. S. Bi, T. Zhao, and B. Luo, Chem. Commun. **48**, 106 (2012).
9. E. Morales-Narváez, B. Pérez-López, L. B. Pires, and A. Merkoci, Carbon **50**, 2987 (2012).
10. Z. Chen, S. Berciaud, C. Nuckolls, T. F. Heinz, and L. E. Brus, ACS Nano **4**, 2964 (2010).
11. L. Gaudreau, K. J. Tielrooij, G. E. D. K. Prawiroatmodjo, J. Osmond, F. García de Abajo, and F. H. L. Koppens, Nano Lett. **13**, 2030 (2013).
12. S. Jander, A. Kornowski, and H. Weller, Nano Lett. **11**, 5179 (2011).
13. R. S. Swathi and K. L. Sebastian, J. Chem. Sci. **121**, 777 (2009).
14. Company data. Retrieved from https://graphene-supermarket.com/Dispersion-in-Water-Single-Layer-Graphene-Oxide-175-ml.html.
15. K. Krishnamoorthy, M. Veerapandian, R. Mohan, and S.-J. Kim, Appl. Phys. A **106**, 501 (2012).
16. M. Pophristic, F. H. Long, C. Tran, I. T. Ferguson, and R. F. Karlicek, Jr., J. Appl. Phys. **86**, 1114 (1999).
17. A. F. van Driel, I. S. Nikolaev, P. Vergeer, D. Vanmaekelbergh, and W. L. Vos, Phys. Rev. B **75**, 035329 (2007).
18. G. Itskos, G. Heliotis, P. G. Lagoudakis, J. Lupton, N. P. Barradas, E. Alves, S. Pereira, I. M. Watson, M. D. Dawson, J. Feldmann, R. Murray, and D. D. C. Bradley, Phys. Rev. B **76**, 035344 (2007).
19. D. M. Kaschak and T. E. Mallouk, J. Am. Chem. Soc. **118**, 4222 (1996).